



Cite this: *Soft Matter*, 2017, 13, 4871

Nanoscopic dynamics of bicontinuous microemulsions: effect of membrane associated protein

V. K. Sharma,^{id}*^a Douglas G. Hayes,^{id}^b Volker S. Urban,^{id}^c Hugh M. O'Neill,^c M. Tyagi^{de} and E. Mamontov^c

Bicontinuous microemulsions (B μ E) generally consist of nanodomains formed by surfactant in a mixture of water and oil at nearly equal proportions and are potential candidates for the solubilization and purification of membrane proteins. Here we present the first time report of nanoscopic dynamics of surfactant monolayers within B μ Es formed by the anionic surfactant sodium dodecyl sulfate (SDS) measured on the nanosecond to picosecond time scale using quasielastic neutron scattering (QENS). B μ Es investigated herein consisted of middle phases isolated from Winsor-III microemulsion systems that were formed by mixing aqueous and oil solutions under optimal conditions. QENS data indicates that surfactants undergo two distinct motions, namely (i) lateral motion along the surface of the oil nanodomains and (ii) localized internal motion. Lateral motion can be described using a continuous diffusion model, from which the lateral diffusion coefficient is obtained. Internal motion of surfactant is described using a model which assumes that a fraction of the surfactants' hydrogens undergoes localized translational diffusion that could be considered confined within a spherical volume. The effect of cytochrome *c*, an archetypal membrane-associated protein known to strongly partition near the surfactant head groups in B μ Es (a trend supported by small-angle X-ray scattering [SAXS] analysis), on the dynamics of B μ E has also been investigated. QENS results demonstrated that cytochrome *c* significantly hindered both the lateral and the internal motions of surfactant. The lateral motion was more strongly affected: a reduction of the lateral diffusion coefficient by 33% was measured. This change is mainly attributable to the strong association of cytochrome *c* with oppositely charged SDS. In contrast, analysis of SAXS data suggested that thermal fluctuations (for a longer length and slower time scale compared to QENS) were increased upon incorporation of cytochrome *c*. This study demonstrates the utility of QENS for evaluating dynamics of B μ Es in nanoscopic region, and that proteins directly affect the microscopic dynamics, which is of relevance for evaluating release kinetics of encapsulated drugs from B μ E delivery systems and the use of B μ Es as biomembrane mimetic systems for investigating membrane protein–biomembrane interactions.

Received 3rd May 2017,
Accepted 10th June 2017

DOI: 10.1039/c7sm00875a

rsc.li/soft-matter-journal

Introduction

Bicontinuous microemulsions (B μ Es, Fig. 1), are self-assembled systems consisting of flexible surfactant monolayers at near-zero

^a Solid State Physics Division, Bhabha Atomic Research Centre, Mumbai 400085, India. E-mail: sharmavk@barc.gov.in; Fax: +91-2225505151; Tel: +91-25594604

^b Department of Biosystems Engineering and Soil Science, University of Tennessee, Knoxville, TN 37996-4531, USA

^c Neutron Sciences Directorate, Oak Ridge National Laboratory, P.O. Box 2008, Oak Ridge, TN 37831-6475, USA

^d NIST Center for Neutron Research, National Institute of Standards, 100 Bureau Dr, Gaithersburg, MD 20899, USA

^e Department of Materials Science and Engineering, University of Maryland, College Park, MD 20742, USA

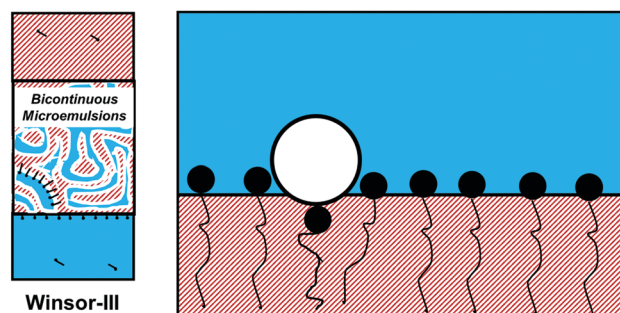


Fig. 1 Schematic diagram of a Winsor-III (W_{III}) system, containing a bicontinuous microemulsion (B μ E) middle phase, and a cartoon representation of cytochrome *c* (as shown by a white circle in the right side sketch) localization within the B μ E system.

curvature separating water and oil nanodomains, and are uniquely suitable for several applications: enhanced oil recovery, templating media for nanoparticles and nanomaterials, blending of polymeric materials, drug delivery, electrochemical analysis, and hosting of multiphase chemical and biochemical reactions.^{1–9} These applications are enabled by B μ Es' unique set of properties: they are isotropic, thermodynamically stable, optically clear, exhibit dynamic motion of constituents and possess nearly equal volume fractions of polar and nonpolar nanodomains separated by a large extent of interfacial area. Therefore, B μ Es allow for co-solubilization of polar, apolar, and amphiphilic substances, and enable good contact between the subphases. Furthermore, their low interfacial curvature supports their utility as biomembrane mimetic systems to investigate membrane protein–biomembrane interactions. We have also used B μ Es for solubilization of membrane-associated proteins and peptides such as cytochrome *c* and melittin.^{10–12}

B μ Es have also been employed by us to extract proteins.^{10,11} Under optimal conditions, where the surfactant's hydrophilic and lipophilic behavior is balanced through control of “tuning parameters” such as salinity or cosurfactant type and concentration, aqueous protein solution and oil/surfactant solution are mixed, forming a three-phase Winsor-III (W_{III}) μ E system consisting of a B μ E middle phase in equilibrium with water and oil “excess” phases (Fig. 1). During such a process, protein originally contained in aqueous media selectively and rapidly partitions into the B μ E phase due to strong interactions between the protein and the surfactant (*e.g.*, electrostatic attraction or hydrophobic interactions), resulting in a B μ E phase highly concentrated in protein (*e.g.*, > 10 g L⁻¹). The protein can then be recovered from the B μ E phase through reduction of the attractive driving force by replacing the aqueous W_{III} bottom phase with an appropriate aqueous stripping solution (*e.g.*, containing a change of pH and/or high salinity).

The goal of this paper is to understand the nanoscopic dynamics of B μ Es. Dynamics of B μ E are believed to be strongly correlated with their viscoelastic properties. Dynamics of surfactant molecules in the self-assembled aggregates can be studied using various experimental techniques such as dynamic light scattering (DLS),^{13–16} nuclear magnetic resonance (NMR)^{17,18} fluorescence correlation spectroscopy (FCS),^{19,20} and inelastic neutron scattering.^{21–29} However, most of these techniques are only capable of observing the dynamics on a limited time and length scales; methods such as pulsed field gradient NMR, DLS, *etc.* tend to measure diffusion on the length scale of over a micrometer and the time scale from micro- to nanoseconds.^{13,30} On the other hand, a microscopic experimental technique such as quasielastic neutron scattering (QENS) is suitable for studying the dynamics of individual surfactant molecules on the time scale from nanoseconds to picoseconds and over the length scale of few Ångströms to nanometers.^{21–26,29} Through QENS, both qualitative and quantitative information can be extracted. Qualitative information refers to the geometrical mechanism of the motion, while quantitative information relates to the correlation times and length scales of the motion. We have successfully employed QENS to study the dynamics of various surfactants in several

different self-assembled structures, from crystalline powder to micelles, to vesicles.^{23–26,29} For a given surfactant, it was found that both the nature and time scale of motion may vary significantly depending on the arrangement of the surfactants in the different types of self-assembled systems. For example, the internal dynamics of sodium dodecyl sulfate (SDS) molecules in micelles at room temperature is described by localized translation diffusion confined within spherical volumes such that the size of confining domain and associated diffusivity increases linearly from its polar head group to its alkyl tail terminus.²³ On the other hand, in the crystalline powder form, only reorientational motion of SDS along the main molecular axis was observed at the ambient temperature.²⁴ However, as the temperature was increased, the fraction of surfactant molecules participating in the reorientational motion increased, and in the chain melt state, SDS molecules underwent localized translational diffusion within spherical volumes, a motion similar to that observed for SDS in micelles.²⁴ One may conclude, therefore, that dynamics in the chain melt state in crystalline powder is similar to that observed in the micelles. Recently, we investigated dynamics of surfactants in catanionic vesicles during the multilamellar to unilamellar transition.²⁶

Here, our aim is to investigate the nanoscopic dynamical behavior of SDS in B μ Es formed using aqueous salt solution, dodecane as oil, and 1-pentanol as cosurfactant, in the presence and absence of cytochrome *c*, using QENS. This information will be useful to assess the release kinetics of solubilized components for drug delivery and recovery of extracted proteins. This investigation will also be important for assessing the nanoscopic behavior of surfactants in B μ Es relative to other biomembrane mimetic systems such as vesicles and micelles, to provide context for comparing thermodynamic and kinetic results between the respective systems. Moreover, the dynamics associated with surfactant-self-assembly systems constitutes a grand challenge requiring a deeper understanding, with utility in paints and coatings, food and cosmetic systems, and oil recovery. This is first report on dynamics of B μ Es on the time scale of nanoseconds to picoseconds and length scale of few Ångströms as studied using QENS technique.

We have also studied the partitioning of cytochrome *c* in the SDS B μ E system through formation of W_{III} systems at neutral pH (*via* an electrostatic attractive driving force), and have found that the incorporation of cytochrome *c* (partitioning of > 70%) leads to the release of water (and to a lesser extent dodecane and pentanol) from the B μ E (*i.e.*, a smaller B μ E volume fraction). Small-angle X-ray scattering (SAXS) results reflect the higher SDS concentration resulting from release of water and oil *via* incorporation of protein and an increase in the degree of ordering of the surfactant monolayer. QENS will provide a deeper understanding of the interaction of cytochrome *c* with B μ Es on a nanoscale.

Materials and methods

Materials

SDS (> 99% pure) was purchased from Avantor Performance Materials (Center Valley, PA, USA). D₂O and NaCl (> 99% pure)

were obtained from Fisher (Pittsburgh, PA, USA). Fully deuterated dodecane, pentanol, and SDS, >98% pure, were purchased from Cambridge Isotopes Laboratories (Tewksbury, MA, USA). Cytochrome *c* from horse heart (dialyzed and lyophilized, MW = 12 000, pI = 10.0–10.5) was obtained from Sigma-Aldrich (St. Louis, MO, USA). *N*-Methyl,*N*-(trimethylsilyl) trifluoroacetamide (MSTFA) (98% pure) containing 1% trichlorosilane was purchased from Campbell Scientific (Rockford, IL, USA). The Coomassie Brilliant Blue G-250[®] protein assay kit, obtained from Pierce (Rockford, IL, USA), was used as recommended by the manufacturer. Deionized water, (18 MΩ × cm), was used throughout.

Methods

Preparation of water/SDS/1-pentanol/dodecane W_{III} systems

W_{III} systems employed for QENS analysis were formed by mixing separate D₂O solutions of salt (with cytochrome *c*) and deuterated or nondeuterated SDS with oil (1-*d*-pentanol/*d*-dodecane, 0.2:1.0 v/v) at room temperature (22.0 ± 1.0 °C) in 20 mL scintillation vials.³¹ The concentration of NaCl, SDS, and cytochrome *c* in the composite aqueous solution prior to W_{III} formation was 2.4% [0.41 M], 3.9% [0.14 M], and 0 g L⁻¹ or 5 g L⁻¹, respectively. The resultant W_{III} system (12–17 mL) contained water and oil at a 1.0/1.2 v/v ratio. For this W_{III} system, α = 0.48 and γ = 0.021, where α is the mass fraction of oil on an SDS-free basis and γ is the mass fraction of surfactant (SDS). The W_{III} systems formed rapidly (typically within 1–2 min); however, to ensure complete phase separation, samples were allowed to equilibrate for at least 6 hours. Thereafter, the middle, BμE, phase was carefully withdrawn through micropipetting and placed firstly in 6 mL scintillation vials for a few hours of equilibration, and then into the QENS sample holders. The isolated BμE phases were optically clear and stable for at least three months. For QENS samples, SDS was the only non-deuterated material in the BμEs, thereby representing a film neutron contrast. To measure the partitioning of SDS and pentanol between the W_{III} phases and the phases' volume fractions, BμE samples were isolated from W_{III} systems prepared on a smaller scale (1–6 mL) using fully hydrogenated materials (water, SDS, pentanol, and dodecane). There were no isotope effects for the SDS/pentanol W_{III} system; moreover, the phase behavior was not affected by use of deuterated *vs.* hydrogenated surfactant or solvents, nor by scale.

Composition analysis of BμE phase

The volume fraction of the three W_{III} phases (φ_{*i*}, where *i* = top, BμE, or bottom) was measured using a ruler calibrated at 1.0 mm intervals after the W_{III} systems were placed in 1 mm path length rectangular quartz cells. The cytochrome *c* concentration was determined by a spectrophotometric assay employed previously.¹⁰ An aliquot of BμE phase (50 μL) was isolated; then 2.0 mL acetone was added (40:1 v/v), to remove the surfactant from the protein and cause precipitation of the protein. Precipitate was isolated and treated with an additional 2.0 mL aliquot of acetone. After undergoing air drying, the

precipitated protein was dissolved in 50 μL of 0.12 M NaCl(aq). Coomassie blue reagent was added to the samples, per the manufacturer's directions, and solution were transferred to 1.0 cm pathlength cuvettes. Absorbance at 595 nm was employed to quantify the protein concentration, using a model UV-1700 spectrophotometer from Shimadzu (Kyoto, Japan). A concentration *vs.* absorbance calibration curve for aqueous BSA standards (Pierce) was employed in the calculations. The concentration of SDS in the phases was measured *via* elemental analysis for atomic sulfur using inductively coupled plasma atomic emission spectrometry. The concentration of pentanol in the top phase was measured *via* gas chromatography (GC), performed using a model QP 2010 GC-MS and a SHR5XLB 30 m × 0.22 mm × 0.25 μm column from Shimadzu. Aliquots from the top W_{III} phase were derivatized *via* silylation, by mixing 50 μL of top phase with 150 μL of hexane and 100 μL of MSTFA solution, and then heating for 20 min at 65 °C. The GC carrier gas was helium at a column flow rate of 1 mL min⁻¹. The GC column temperature program oven temperature: an initial isothermal hold at 35 °C for 3 min, followed by a gradient of 5 °C min⁻¹ to 50 °C and a second gradient of 50 °C min⁻¹ to 300 °C, followed by a 2 minute hold at 300 °C. The injector temperature was held at 225 °C. The mass spectrometer employed 30–200 *m/z* and was operated at 260 °C. For the MS detector the temperature of the ion source and the interface were 260 °C and 250 °C, respectively, in scan mode from 30 *m/z* to 200 *m/z*. Volume fractions of water, oil (dodecane), SDS, and cosurfactant (pentanol) in the middle phase (φ_w, φ_o, φ_s, and φ_c, respectively) were determined *via* mass balances, assuming that water and dodecane/pentanol were immiscible.

Small-angle X-ray scattering (SAXS) measurements

BμE phases in the presence and absence of 5 g L⁻¹ (aq) of cytochrome *c* were investigated *via* SAXS at room temperature using a BioSAXS2000 instrument from Rigaku (The Woodlands, TX, USA), which employs a copper anode X-ray source (wavelength of 1.5418 Å) and covers a *Q* range of 0.01–0.70 Å⁻¹. Data were normalized and reduced according to the manufacturer's recommendations. SAXS data were fit near the maximum of the scattering curve (*Q* = *Q*_{max}) using the Teubner–Strey (T–S) model, which is commonly used for BμEs.³² This model provides as outputs the quasiperiodic repeat distance (*d*), the correlation length (ξ) as outputs. The former refers to the average length across two adjacent water and oil nanodomains and ≈ 2π/*Q*_{max}. ξ is inversely related to the width of the scattering peak, and to the surface area per volume of the surfactant monolayer in the BμE phase:³²

$$S/V = 4\phi_w\phi_o\xi^{-1} \quad (1)$$

Quasielastic neutron scattering (QENS) measurements

QENS experiments were carried out at the National Institute of Standards and Technology (NIST) Center for Neutron Research using the cold neutron time-of-flight Disc Chopper Spectrometer (DCS). DCS is a direct geometry time of flight spectrometer, which employs seven synchronized disk choppers spinning at

high speed to produce a pulsed monochromatic neutron beam.³³ QENS experiments have been carried out on SDS B μ E in film neutron contrast with and without cytochrome *c*. In film contrast, except for SDS, all other constituents (such as water, oil) of B μ E are deuterated. It should be noted that cytochrome *c* is also protonated, but added in a very small amount, 1/1000 of the number of SDS molecule. Scattering contribution of cytochrome *c* would be about 3% of the total measured scattering. The incident neutron wavelength $\lambda = 6.0 \text{ \AA}$ was selected. At this wavelength ($E_i = 2.27 \text{ meV}$) and for the high intensity resolution mode of the instrument, *Q*-averaged energy resolution of full width half maximum (FWHM) of the spectrometer is about 65 \mu eV . This configuration resulted in a wave vector (*Q*) transfer range of $0.5\text{--}1.9 \text{ \AA}^{-1}$. To estimate the solvent contributions to the scattering, QENS measurements were also carried out on fully deuterated SDS B μ E. All QENS measurements were carried out at $25 \text{ }^\circ\text{C}$. For QENS experiments, B μ E solutions were placed in the annular aluminum sample holders or cans, sealed with an indium O-ring and mounted on a closed-cycle refrigerator. The temperature was controlled within $\pm 0.1 \text{ }^\circ\text{C}$. The inner diameter of the outside can was 19.9 mm , and the outer diameter of inside can was 19.0 mm , yielding a sample volume of $\sim 2.7 \text{ mL}$ and a sample thickness of 0.45 mm . This gives no more than 10% scattering from the B μ E samples, thereby minimizing multiple scattering effects. Sample cans containing the B μ E samples were weighed before and after QENS measurements, to confirm the absence of weight loss due to leakage and evaporation. For instrument resolution and detector normalization, QENS experiments have also been carried out on a vanadium standard. The package MSLICE of the Dave software,³⁴ developed by NIST, was used to carry out standard data reduction, which includes background subtraction and detector efficiency corrections.

Results and discussion

Composition of the B μ E solutions

Compositional information on the resultant B μ E solutions is given in Table 1. In the absence of cytochrome *c*, the B μ E phase consists of 50 (vol)% water and 45% dodecane + pentanol. The addition of cytochrome *c* reduced the B μ E phase volume fraction, $\phi_{\text{B}\mu\text{E}}$, from 0.32 to 0.23, and changed the B μ E composition to 32% water and 61% dodecane + pentanol, reflecting that the B μ E surfactant monolayers became more lipophilic. The cytochrome *c* addition also increased the SDS (and pentanol) volume fractions in the B μ E phase from 0.05 to 0.07 (from 0.13 to 0.18). The resultant cytochrome *c* concentration in the B μ E phase, 7.2 g L^{-1} , occurred due to the high (73%) partitioning of the protein to the B μ E phase.

Small-angle X-ray scattering results

SAXS was employed to obtain structural information on the B μ Es in the presence and absence of cytochrome *c*. The shape of the scattering curve, with a peak at low *Q*, is typically encountered with B μ Es³² as is simulated effectively by the T–S model [Fig. 2(a)]. The addition of cytochrome *c* leads to a major

Table 1 Compositional information and parameters derived from the Teubner–Strey (T–S) model fit of the SAXS data for the B μ E phases within the water/SDS/pentanol/dodecane W_{III} system with and without cytochrome *c* (5 g L^{-1} in original aqueous solution) at $T = 22.0 \pm 1.0 \text{ }^\circ\text{C}$ ^{a,b}

Symbol	No protein	Cytochrome <i>c</i>
$[\text{P}]_{\text{B}\mu\text{E}}, \text{ g L}^{-1}$	0.0	7.1 ± 0.2
$\phi_{\text{B}\mu\text{E}}$	0.32 ± 0.00	0.23 ± 0.01
ϕ_{w}	0.50 ± 0.00	0.32 ± 0.03
ϕ_{o}	0.32 ± 0.02	0.43 ± 0.03
ϕ_{s}	0.05 ± 0.01	0.07 ± 0.01
ϕ_{cs}	0.13 ± 0.01	0.18 ± 0.02
$d, \text{ \AA}$	267.7 ± 0.0	206.3 ± 0.0
$\xi, \text{ \AA}$	86.1 ± 0.0	69.2 ± 0.0
$S/V, \text{ \AA}^{-1} \times 1000$	10.5 ± 0.5	11.4 ± 1.2
$a_0, \text{ \AA}^2$	97.0 ± 11.5	78.5 ± 11.6
$\kappa_{\text{theor}}/k_{\text{B}}T$	0.881 ± 0.000	0.831 ± 0.000

^a Row headings: $[\text{P}]_{\text{B}\mu\text{E}}$ = protein concentration in the resultant B μ E phase; $\phi_{\text{B}\mu\text{E}}$ volume fraction of B μ E phase within the W_{III} system; ϕ_{w} , ϕ_{o} , ϕ_{s} , and ϕ_{cs} = volume fraction of water, oil (dodecane), surfactant, and cosurfactant in the B μ E phase, respectively; d , ξ , S/V , a_0 , and κ_{theor} refer to the quasi-periodic repeat distance, correlation length, surface area per volume of surfactant monolayers, surface area per surfactant head group, and theoretical bare bending elasticity constant, respectively (derived from Teubner–Strey [T–S] model fitting of the SAXS data); k_{B} refers to Boltzmann's constant. ^b The volume fraction of protein is negligible (≤ 0.005).

change of the scattering curve: a shift of the scattering curve to higher *Q* and a broadening of the curve, reflecting a decrease of d and ξ . These trends are consistent with the lower values of d and ξ obtained for B μ Es containing cytochrome *c* through T–S model fitting (Table 1). These trends reflect the increase of SDS concentration in the B μ E phase (ϕ_{s}) upon incorporation of cytochrome *c* due to the release of water and oil. To determine the underlying cause of the changes in structure observed by SAXS, the surface area per surfactant head group (a_0) was calculated:

$$a_0 = \frac{v_s}{\phi_s} \frac{S}{V} \quad (2)$$

where v_s is the volume per SDS molecule (465 \AA^3). The addition of cytochrome *c* led to a major decrease of a_0 , 18.5 \AA^2 (Table 1), suggesting the ability of SDS to lower interfacial tension between aqueous and apolar B μ E subphases was greatly reduced. A similar trend was observed during the W_{III} extraction of proteins possessing strong positive charges (*i.e.*, proteins with high pI) by the anionic surfactant sodium dioctyl sulfosuccinate (AOT), and was attributed to strong electrostatic attractive binding between the proteins and surfactant head groups.¹¹

T–S-derived parameters can be combined to calculate the theoretical bare bending elasticity constant, κ_{theor} :^{27,35–37}

$$\frac{\kappa_{\text{theor}}}{k_{\text{B}}T} = \frac{5\sqrt{3}}{64} \frac{2\pi\xi}{d} + \frac{3}{4\pi} \ln\left(\frac{d}{2l_s}\right) \quad (3)$$

where k_{B} and l_s refer to Boltzmann's constant and the length of the surfactant monolayer, respectively. The latter is estimated to be 10.5 \AA , derived from Porod analysis of small-angle neutron scattering data for the same W_{III} system.¹² The first term of

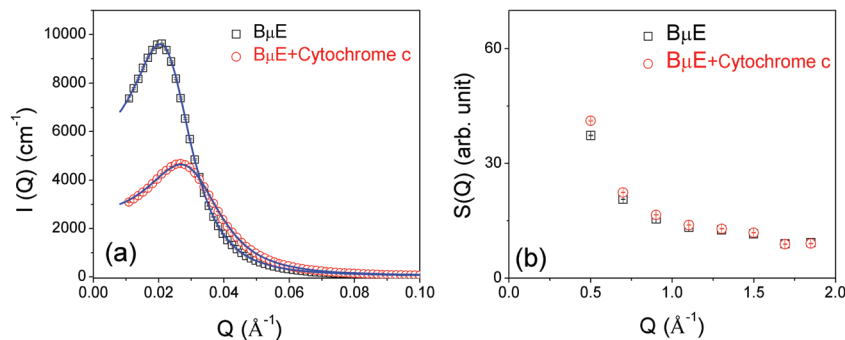


Fig. 2 (a) Small-angle X-ray data for B μ E in the absence and presence of cytochrome *c* (5.0 g L $^{-1}$ of aqueous phase used to form W $_{III}$ system) at 22 °C. Solid lines represent Teubner–Strey model fits to the data. Error bars for $I(Q)$ fall within the symbols contained in the figure. (b) The structure factor $S(Q)$, obtained by integration of the QENS data over energy transfer.

eqn (3) represents the renormalized bending modulus, describing membrane fluctuations up to the B μ E characteristic length scale, d , and is directly related to the saddle-splay and intrinsic bending moduli for the bare surfactant interface. The second term of eqn (3) serves as a renormalization correction term. As shown in Table 1, the addition of cytochrome *c* slightly decreased κ_{theor} , suggesting the protein promoted an increase of interfacial fluidity, hence thermal fluctuations. The increased fluidity is likely a result of the decreased extent of ordering for SDS at the interface of oil and water nanodomains, as described above.

Quasielastic neutron scattering results

Neutrons have large incoherent scattering cross section by hydrogen (H) compared to coherent or incoherent scattering cross sections by its isotope deuterium (D) or other elements (C, O, N, S) present in the current system. This enables us to distinguish the dynamics of surfactants from those of solvent through isotopic sensitivity. QENS measurements have been carried out in film contrast; *i.e.*, only SDS is non-deuterated and the other components, water, oil and co-surfactant, are deuterated. To remove the finite contribution from the deuterated solvents, QENS measurements were also carried out on fully deuterated B μ Es (including d-SDS), and the scattered intensity for this sample was subtracted from QENS data for the film contrast B μ Es. It is noted that scattering contribution of d-SDS is approximately an order of magnitude smaller than protonated SDS and hence neglected here. Therefore, background-subtracted QENS spectra mainly reflect the dynamics of h-SDS in B μ Es. In order to evaluate the influence of the incorporated cytochrome *c* on the structure of B μ E at the length scale relevant to QENS, the structure factor, $S(Q)$, was obtained by integration of the QENS data over energy transfer, and shown in Fig. 2(b). The data demonstrate very limited influence of cytochrome *c* on the structure factor. Representative QENS spectra for SDS B μ Es are shown in Fig. 3 at two different Q values. Instrument resolution as measured using standard vanadium is overlaid in the figure to serve as a reference. QENS spectra for all samples were normalized through dividing data by the peak amplitude, $S(Q,0)$. Significant quasielastic broadening is observed for SDS B μ Es, indicating stochastic dynamics of SDS in the B μ Es. To investigate effect of an archetypal membrane protein on the dynamics of biomembrane-mimetic B μ Es, a small amount of

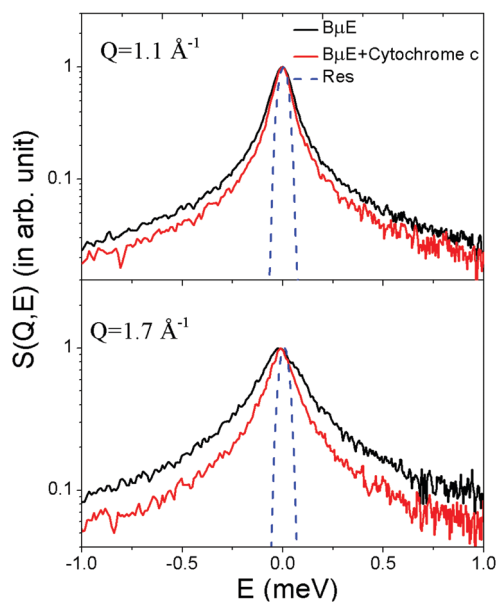


Fig. 3 Representative QENS spectra for SDS B μ Es with and without cytochrome *c* at two different Q values. The contribution of the solvent has been subtracted. For direct comparison of quasielastic broadening for B μ Es in the presence and absence of cytochrome *c*, spectra were normalized by dividing the value of peak amplitudes $S(Q,0)$. The instrument resolution ("Res") is shown by the dashed lines.

cytochrome *c* (~ 0.1 mol%) was incorporated in the B μ Es. It is evident from Fig. 3 that incorporation of cytochrome *c* decreased the quasielastic broadening, indicating hindrance of the dynamics of B μ E by cytochrome *c*. As mentioned earlier, scattering contribution of the cytochrome *c* in the measured scattering spectra would be $\sim 3\%$ which is rather small, especially considering the magnitude of the observed effects. Hence, the observed changes in the scattering spectra are predominantly not due to superposition of surfactant and protein dynamics, but due to impact of protein on the surfactant dynamics. The QENS data therefore indicates that cytochrome *c* acts as a stiffening agent, restricting the observed dynamics of SDS in the B μ Es. This trend contrasts the increase of thermal fluctuations (decrease of κ_{theor}) observed upon the incorporation of cytochrome *c* through SAXS analysis (Table 1). The difference is attributable to the dynamics observed

on different time and length scale. By SAXS, we extract bending modulus corresponding to undulation motion which occurs on a larger length ($\sim \mu\text{m}$) and a slower time scale (μs to ns). On the other hand, QENS mainly observes motions on the length scale of few Angstroms to nanometer and time scale of picoseconds to nanoseconds. The hindrance of short-range dynamics by cytochrome *c* is likely due to the strong electrostatic attractive binding between the positively-charged protein and the negatively-charged SDS, a trend supported by SAXS analysis.

A unique capability of QENS is to deduce the geometry as well as time scale of the relaxation processes for surfactants existent in the B μ Es. The geometry of the relaxation process is obtained from the Q -dependence of the scattering signal. A Q -dependent broadening is characteristic of the long-range translational diffusion, while a Q -independent width is a signature of the localized motion. Surfactants in the B μ Es can undergo different kinds of motion, such as vibrational, torsional, conformational, rotation, lateral, and undulation, which cover a broad range of time scales, from femtoseconds for molecular vibrations, to a few tens of nanoseconds for the undulation, and a wide range of length scales, from a few tens of nanometers for undulation modes of the surfactant film, to Ångströms for local surfactant molecule motions.^{27,38–40} QENS is a technique suitable for studying the motion of individual amphiphile molecules on the nanosecond to picoseconds time scale.^{22–26,29} The present configuration of neutron spectrometer (energy resolution $\Delta E = 65 \mu\text{eV}$, corresponding to observation time of 20 ps, calculated as $\Delta E = 2\hbar/\tau_{\text{obs}}$, and energy transfer range suitable for data analysis of -2 meV to $+1.0 \text{ meV}$) allows investigation of motion in the range of time scale from 0.5 ps to 20 ps. On this time scale, we can expect two different kinds of motions to contribute to the measured QENS spectra, namely, the lateral motion of the whole surfactant along the surface of the nanochannels and the internal motion of surfactant. As a first approximation, it is assumed that both lateral and internal motions are independent of each other, resulting in the following scattering law²¹

$$S_{\text{B}\mu\text{E}}(Q, E) = [S_{\text{lat}}(Q, E) \otimes S_{\text{int}}(Q, E)] \quad (4)$$

where $S_{\text{lat}}(Q, E)$ and $S_{\text{int}}(Q, E)$ are the scattering laws correspond to lateral and internal motions of the surfactant molecules, respectively. For the truly two-dimensional lateral motion, the powder-averaged scattering law featuring a logarithmic singularity at zero energy transfer⁴¹ would have to be computed numerically. However, it turns out that the regular scattering law for three-dimensional motions describes the data quite well, consistent with the model used in the literature on the various similar model membrane system.^{26,42–44} The applicability and successful use of the 3D diffusion model is likely attributable to the fact that neither the surface of B μ E/membrane is perfectly planar (two-dimensional), nor does diffusion of the surfactant take place thoroughly in the plane, as the surfactant can undergo small diffusion motion (up and down) normal

to plane. Therefore, for lateral motion, the scattering law can be written as follows:²¹

$$S_{\text{lat}}(Q, E) = L_{\text{lat}}(\Gamma_{\text{lat}}, E) = \frac{1}{\pi} \frac{\Gamma_{\text{lat}}}{\Gamma_{\text{lat}}^2 + E^2} \quad (5)$$

where Γ_{lat} is the half width at half maxima (HWHM) of the Lorentzian corresponding to the lateral motion. Internal motion of SDS is locally restricted per the chemical structure of the surfactant molecule, and hence should be localized in character. Therefore, the scattering law for internal motion of the surfactant molecules can be described by:²¹

$$S_{\text{int}}(Q, E) = [A(Q)\delta(E) + (1 - A(Q))L_{\text{int}}(\Gamma_{\text{int}}, E)] \quad (6)$$

where the first term represents the elastic component and second term represents the quasielastic component, approximated by a single Lorentzian function, $L_{\text{int}}(\Gamma_{\text{int}}, E)$ with a half width at half maximum (HWHM), Γ_{int} . $A(Q)$ is known as Elastic Incoherent Structure Factor (EISF) which is the fraction of the elastic scattering with respect to the total scattering. Hence, from eqn (4–6), the scattering law for B μ Es can be written as a sum of two Lorentzian functions:

$$S_{\text{B}\mu\text{E}}(Q, E) = L_{\text{lat}}(\Gamma_{\text{lat}}, E) \otimes [A(Q)\delta(E) + (1 - A(Q))L_{\text{int}}(\Gamma_{\text{int}}, E)] \\ = A(Q)L_{\text{lat}}(\Gamma_{\text{lat}}, E) + (1 - A(Q))L_{\text{tot}}(\Gamma_{\text{tot}}, E) \quad (7)$$

Here the Lorentzian, $L_{\text{tot}}(\Gamma_{\text{tot}}, E)$ represents the combination of lateral and internal motions of the surfactant, where $\Gamma_{\text{tot}} = \Gamma_{\text{lat}} + \Gamma_{\text{int}}$. For the data fitting, the scattering law model, as given by eqn (7), is convoluted with the instrumental resolution function, and the parameters $A(Q)$, Γ_{lat} and Γ_{tot} are determined by least-squares fitting of the measured spectra. The fitting procedure has been performed for each Q value independently. The scattering law as given in eqn (7) describes well the observed QENS spectra for B μ Es in the absence and presence of cytochrome *c* at all the Q values, as evidenced by the excellent model fits shown for both B μ Es at two different Q values in Fig. 4. It is noteworthy that no model for Q dependence is assumed *a priori* during the fitting, neither for the weight factors, nor for the width of the Lorentzian functions. Hence, the variations of the fit parameters $A(Q)$, Γ_{lat} and Γ_{tot} with Q resulting from the fit can be used to verify the theoretical models.

Lateral motion

The Q dependence for the HWHM of the Lorentzian corresponding to lateral motion, Γ_{lat} , for SDS B μ Es with and without cytochrome *c* is shown in Fig. 5. It is found that for both B μ Es, Γ_{lat} increased linearly with Q^2 , indicating that the lateral motion of surfactant is a continuous diffusion process.²¹ It is evident from Fig. 5 that Γ_{lat} , hence the extent of lateral motion for SDS in the presence of cytochrome *c*, is consistently lower than in protein-free B μ Es, indicating hindrance in the lateral motion due to addition of cytochrome *c*. The linear relationship between Γ_{lat} and Q^2 exhibited in Fig. 5 reflects the applicability of Fick's law, $\Gamma_{\text{tot}} = \hbar D_{\text{lat}} Q^2$, where D_{lat} refers to the lateral

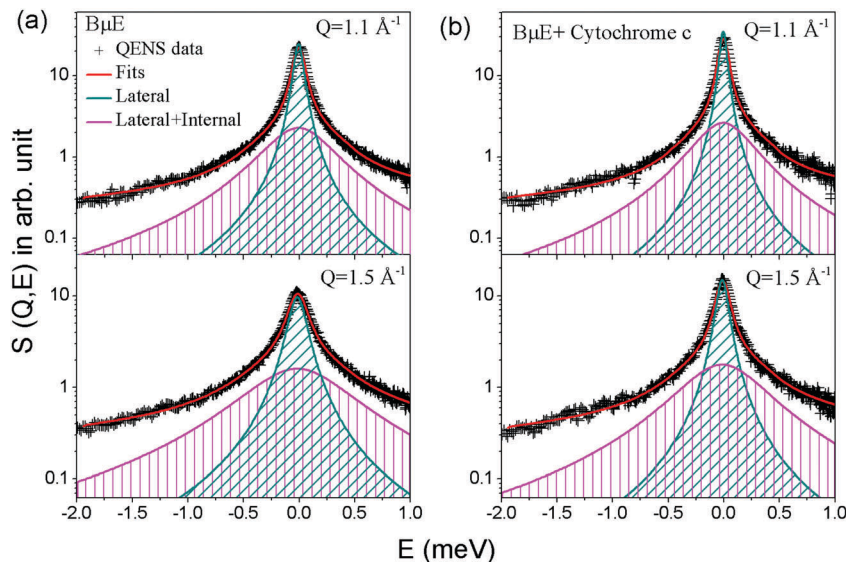


Fig. 4 Typical fitted QENS spectra for B μ E's in the (a) absence and (b) presence of cytochrome *c* at 25 °C, based on eqn (7).

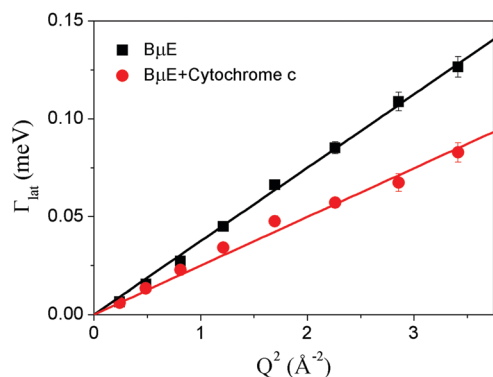


Fig. 5 Variation of HWHM of first Lorentzian (Γ_{lat}) (obtained from model fitting of eqn (7) to the QENS data, per Fig. 4) corresponding to lateral motion of SDS in B μ E's in the absence and presence of cytochrome *c*. Solid lines correspond to the fit of Fick's Law of diffusion to the data. Error bars throughout the text represent one standard deviation.

diffusion coefficient of SDS. Values of D_{lat} for SDS in B μ E's formed in the absence and presence of cytochrome *c*, are found to be $5.7 \pm 0.1 \times 10^{-6} \text{ cm}^2 \text{ s}^{-1}$ and $3.8 \pm 0.1 \times 10^{-6} \text{ cm}^2 \text{ s}^{-1}$, respectively, reflecting a 33% decrease of diffusivity induced by the protein. Lateral motion of SDS along the surfactant monolayers separating the water and oil nanodomains would be significantly restricted due to the presence of protein near the surfactant head groups, which likely occurred, per the SAXS analysis of the data described above (Fig. 1). It is of interest to investigate effects of geometry of aggregates (spherical, lamellar, *etc.*) on the lateral diffusion coefficient of the surfactants, to compare with other QENS studies of surfactants in different self-assembled structures, *e.g.*, vesicles and micelles.^{15,26} The nanoscopic dynamics of surfactants in cationic vesicles based on SDS/CTAB (cetyl trimethyl ammonium bromide) has been studied to investigate effect of multilamellar to unilamellar transition.²⁶ It was found that fraction of surfactant molecules

undergoing lateral diffusion increased by a factor of 2 when vesicles underwent the multilamellar to unilamellar transition. At 300 K, D_{lat} of surfactants in unilamellar phase was found to be $3.0 \times 10^{-6} \text{ cm}^2 \text{ s}^{-1}$. The dynamics of SDS in micelles has also been investigated, and at 300 K, D_{lat} was found to be $3.4 \times 10^{-6} \text{ cm}^2 \text{ s}^{-1}$.²⁵ It should be noted that a direct quantitative comparison of the lateral diffusion coefficients of surfactants is not straightforward, since the dynamics of surfactant may depend on various factors such as temperature, concentration of surfactants and electrolytes, and the resolution of the spectrometer used in different studies. However, qualitatively, lateral diffusion of SDS in B μ E, lamellae or micelles seems to be very similar, and Fickian in character, suggesting that the geometry of the aggregate does not influence the diffusion to any significant extent. This result is consistent with an earlier NMR study⁴⁵ that compared diffusivities of surfactant for several different self-assembly structures, indicating that structure of aggregates has negligible effect on the lateral motion of surfactants.

Internal motion

As discussed earlier, a relatively fast internal motion is also observed along with the lateral motion. Internal motion of SDS surfactant can be characterized by the EISF $A(Q)$ and Γ_{int} . The width corresponding to the internal motion, Γ_{int} is obtained by the subtraction of Γ_{lat} from the width of 2nd Lorentzian, Γ_{tot} . The $A(Q)$ and $\Gamma_{\text{int}}(Q)$ for B μ E's in the absence and presence of cytochrome *c* at different Q values are shown in Fig. 6(a) and (b), respectively. It is evident from Fig. 6(b) that for both B μ E's at low Q , Γ_{int} is nearly constant; therefore, as $Q \rightarrow 0$, Γ_{int} is likely to remain nonzero. However, at higher Q , Γ_{int} increases with Q . This is a typical signature of localized translational diffusion within a spherical volume.^{21,46} At lower Q ($QR < \pi$; where R is radius of confining spherical domain), *i.e.*, when larger distances are probed, the behavior of Γ_{int} is independent of Q .

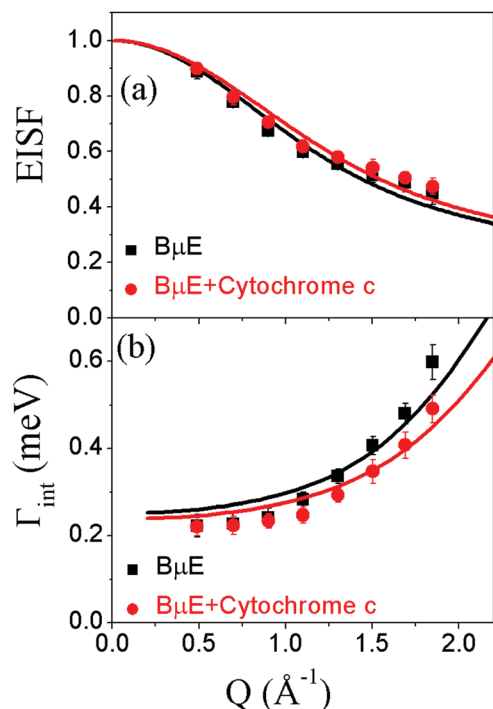


Fig. 6 Variation of (a) EISF $A(Q)$ and (b) HWHM of Lorentzian corresponding to internal motion, Γ_{int} for SDS B μ E with and without cytochrome *c*. Solid lines are the fits as per localized translational diffusion within a spherical volume, as described in the text (eqn (8) and (9)).

This is because at these length scales, hydrogen atoms of SDS molecule are seen to engage in localized dynamics. Therefore, behavior of the quasielastic width in this Q range resembles that of the rotational motion. However, at larger Q values ($QR > \pi$), where small distances are probed, the usual DQ^2 behavior corresponding to translational motion in an infinite medium is recovered, because on this length scale, the confining domain effects of wall boundaries are not yet seen by the diffusing particles. Internal motion of surfactants is complex and comprises various localized motions including reorientational, conformational, torsional and so forth. However, it is not possible to isolate all of these motions and model them individually using data sets with finite energy resolution and limited energy-transfer range. It has been assumed that, as an effective superposition of all these motions, hydrogen atoms in SDS molecules undergo localized translational diffusion confined within a spherical volume. Furthermore, it is possible that all the hydrogen atoms in the alkyl chain may not be dynamically active at a given temperature. Hence EISF can be written as^{21,46}

$$A(Q) = p_x + (1 - p_x) \left[\frac{3j_1(QR)}{QR} \right]^2 \quad (8)$$

where p_x is the fraction of hydrogen atoms that are immobile on the observation time scale, j_1 is the first-order spherical Bessel function, and R is the radius of the confining sphere. It is found that eqn (8) describes well the observed EISF, $A(Q)$, for B μ E with

and without cytochrome *c*, as shown by solid lines in the Fig. 6(a).

For SDS B μ E in the absence of cytochrome *c*, the fraction of mobile hydrogen, $(1 - p_x)$ and R are found to be 53% and $2.3 \pm 0.1 \text{ \AA}$, respectively. The results indicate that, on average, about 53% of hydrogens belonging to alkyl chain undergo localized translation diffusion within a sphere of radius of 2.3 \AA . It is found that addition of 0.1 mol\% cytochrome *c* did not greatly affect the fraction of mobile hydrogens and radius of confining sphere; $(1 - p_x)$ and R were found to be 51% and $2.1 \pm 0.1 \text{ \AA}$, respectively.

For any model to be considered reliable, it should simultaneously describe both EISF and HWHM that correspond to internal motions. The scattering law for localized translational diffusion described above can be written as:⁴⁶

$$S_{\text{int}}(Q, E) = \left[p_x + (1 - p_x) \left[\frac{3j_1(QR)}{QR} \right]^2 \right] \delta(\omega) + (1 - p_x) \left[\frac{1}{\pi} \sum_{\{l,n\} \neq \{0,0\}} (2l+1) A_n^l(QR) \frac{\hbar(x_n^l)^2 D_{\text{int}} / R^2}{\left[\hbar(x_n^l)^2 D_{\text{int}} / R^2 \right]^2 + E^2} \right] \quad (9)$$

where $A_n^l(QR)$ ($n \neq 0$; $l \neq 0$) is the quasielastic structure factor. Its values for different n and l can be calculated using the values of x_n^l .⁴⁶ Here D_{int} is the diffusion coefficient for internal motion. No analytical expression exists for the HWHM of the quasielastic part, in contrast to EISF, for which HWHM can be calculated numerically [using eqn (9)] for given values of p_x , R and D_{int} . The least-squares fitting method is used to describe the observed Γ_{int} with D_{int} as a parameter, while the values of p_x and R are already known from the fit of the EISF. It is found that the localized translational diffusion model [eqn (9)] describes the HWHM of the Lorentzian well, with HWHM corresponding to internal motion for B μ E with and without cytochrome *c* as shown in Fig. 6(b). In the absence and presence of cytochrome *c*, D_{int} was found to be $4.8 \pm 0.1 \times 10^{-5} \text{ cm}^2 \text{ s}^{-1}$ and $4.1 \pm 0.1 \times 10^{-5} \text{ cm}^2 \text{ s}^{-1}$, respectively, suggesting that addition of cytochrome *c* modestly reduces the internal motion of SDS (by 15%). The decrease in D_{int} by cytochrome *c* would likely occur as a result of the partitioning of cytochrome *c* near the polar head groups of SDS in the B μ E monolayers. Internal motions mainly involve the local motion of the alkyl chains, which would not experience as much interaction with cytochrome *c* as lateral motions. However, for lateral motion, which involves whole SDS molecules along the surfactant monolayers exposed to the oil subphase, the effect of cytochrome *c* is more prominent. Recently we have carried out neutron scattering studies to understand the interaction mechanism with phospholipid bilayers of different additives including membrane-active peptides, vitamins, cholesterol, and non-steroid anti-inflammatory drugs.^{47–51} Based on our findings, we hypothesize that there is a strong correlation between the changes in nanoscopic dynamics behavior of biomembranes with the location of additives within the system. It is found that

additives that partition to the head group or biomembrane interface (e.g., melittin and alamethicin) are more prone to affect the slower lateral motion, which involves whole lipid molecules motion along the leaflet, with no significant effect on the faster internal motion. On the other hand, if additive is located well within the biomembrane core (e.g., hydrophobic additives such as cholesterol and vitamin E), they affect both the lateral and internal motions of the membrane. It has been shown that effects of additive strongly depend on the phase and composition of the bilayer. For example, for the solid gel phase, melittin is found to enhance the lateral motion by acting as a plasticizer; but for fluid phases it acts as a stiffening agent. The results of the current study support our hypothesis, as cytochrome *c*, affecting predominately the lateral motion, is found near the head group.

Conclusions

Quasielastic neutron scattering reveals the nature of nanoscopic dynamics of the surfactant SDS in B μ Es formed in the presence and absence of the membrane-associated protein cytochrome *c* on the range of time scales of picoseconds to nanoseconds. The B μ Es have been formed using hydrogenated SDS and deuterated water, oil (dodecane), and cosurfactant (1-pentanol), *i.e.*, a film contrast. Two distinct motions, namely lateral and internal motion, of SDS have been observed. Lateral motion is well described by Fick's Law of diffusion, whereas internal motion is modeled by assuming localized translational diffusion within a spherical volume. The presence of cytochrome *c* has decreased the lateral diffusivity by 33% and the internal motion diffusivity to a lesser extent (15%). These trends are consistent with additives that bind directly with the head groups of surfactants, as supported by SAXS analysis of SDS, and are in contrast to the increase of thermal fluctuations by cytochrome *c* observed through SAXS analysis. The contrasting trends for the incorporation of cytochrome *c* between QENS and SAXS are likely due to difference in the length and time scales probed, with the former focusing upon a smaller length scale and faster time scale. This study therefore demonstrates that additives that interact with surfactants can have a direct impact on the short-range dynamics, and that trends observed for vesicles, micelles, and other surfactant self-assembly systems relate also to B μ Es. Furthermore, the decrease of short-range diffusion for surfactants due to ion-paired additives such as proteins may affect the kinetics of the release of the additives, thereby affecting several different potential applications of B μ Es, such as protein purification, drug delivery, and enhancement of oil recovery.

Acknowledgements

The research was financially supported by the Laboratory Directed Research and Development program of Oak Ridge National Laboratory. Measurement of pentanol and SDS concentrations were conducted by Ms Galina Melnichenko

(Biosystems Engineering Department, University of Tennessee) and Galbraith Laboratories (Knoxville, TN, USA), respectively. Matthew J. Cuneo (Biology and Soft Matter Division, Oak Ridge National Laboratory) is acknowledged for his assistance in collecting the SAXS data. This work utilized facilities supported in part by the National Science Foundation under Agreement No. DMR-1508249. Certain commercial material suppliers are identified in this paper to foster understanding; such identification does not imply recommendation or endorsement by NIST. Certain commercial material suppliers are identified in this paper to foster understanding; such identification does not imply recommendation or endorsement by NIST.

References

- 1 D. G. Hayes, in *Liposomes, Lipid Bilayers, and Model Membranes: from Basic Research to Application*, ed. G. Pabst, N. Kucerka, M. P. Nieh and J. Katsaras, CRC Press, 2014, pp. 179–198, ch. 10.
- 2 M. Kunitake, E. Kuraya, D. Kato, O. Niwa and T. Nishimi, *Curr. Opin. Colloid Interface Sci.*, 2016, **25**, 13–26.
- 3 D. Johnson, F. Galiano, S. A. Deowan, J. Hoinkis, A. Figoli and N. Hilal, *J. Membr. Sci.*, 2015, **484**, 35–46.
- 4 S. Vargas-Ruiz, O. Soltwedel, S. Micciulla, R. Sreij, A. Feoktystov, R. von Klitzing, T. Hellweg and S. Wellert, *Langmuir*, 2016, **32**(45), 11928–11938.
- 5 R. Latsuzbaia, E. Negro and G. Koper, *Faraday Discuss.*, 2015, **181**, 37–48.
- 6 J. L. Salager, A. M. Forgiarini, R. E. Anton and L. Quintero, *Energy Fuels*, 2012, **26**, 4078–4085.
- 7 B. H. Jones and T. P. Lodge, *Chem. Mater.*, 2010, **22**, 1279–1281.
- 8 P. A. Reyes, J. A. Espinoza, M. E. Treviño, H. Saade and R. G. López, *J. Nanomater.*, 2010, 948941.
- 9 D. Langevin, *Annu. Rev. Phys. Chem.*, 1992, **43**, 341–369.
- 10 J. A. Gomez del Rio and D. G. Hayes, *Biotechnol. Prog.*, 2011, **27**, 1091–1100.
- 11 D. G. Hayes, J. A. Gomez del Rio, Y. Ran, V. S. Urban, S. V. Pingali and H. M. O'Neill, *Langmuir*, 2015, **31**(6), 1901–1910.
- 12 D. G. Hayes, Y. Ran, R. N. Dunlap, D. B. Anunciado, S. V. Pingali, H. M. O'Neill and V. S. Urban, *Biochim. Biophys. Acta, Biomembr.*, 2017, under review.
- 13 P. A. Hassan, S. Rana and G. Verma, *Langmuir*, 2015, **31**, 3–12.
- 14 M. Mihailescu, M. Monkenbusch, H. Endo, J. Allgaier, G. Gompper, J. Stellbrink, D. Richter, B. Jakobs, T. Sottmann and B. Farago, *J. Chem. Phys.*, 2001, **115**, 9563–9577.
- 15 T. L. Morkved, B. R. Chapman, F. S. Bates, T. P. Lodge, P. Stepanek and K. Almdal, *Faraday Discuss.*, 1999, **112**, 335–350.
- 16 S. Wellert, M. Karg, O. Holderer, A. Richardt and T. Hellweg, *Phys. Chem. Chem. Phys.*, 2011, **13**, 3092–3099.
- 17 M. F. Roberts and A. G. Redfield, *J. Am. Chem. Soc.*, 2004, **126**, 13765–13777.

- 18 P. J. Bratt, D. G. Gillies, L. H. Sutcliffe and A. J. Williamst, *J. Phys. Chem.*, 1990, **94**, 2727–2729.
- 19 R. Macháň and M. Hof, *Biochim. Biophys. Acta*, 2010, **1798**, 1377–1391.
- 20 R. Neubauer, S. Höhn, M. Dulle, A. Lapp, C. Schulreich and T. Hellweg, *Soft Matter*, 2017, **13**(10), 1998–2003.
- 21 M. Bée, *Quasielastic Neutron Scattering*, Adam Hilger, Bristol, 1988.
- 22 M. Freda, G. Onori, A. Paciaroni and A. Santucci, *Phys. Rev. E: Stat., Nonlinear, Soft Matter Phys.*, 2003, **68**, 0214061.
- 23 V. K. Sharma, S. Mitra, G. Verma, P. A. Hassan, V. Garcia Sakai and R. Mukhopadhyay, *J. Phys. Chem. B*, 2010, **114**, 17049–17056.
- 24 S. Mitra, V. K. Sharma, V. Garcia Sakai, J. P. Embs and R. Mukhopadhyay, *J. Phys. Chem. B*, 2011, **115**(32), 9732–9738.
- 25 V. K. Sharma, S. Mitra, M. Johnson and R. Mukhopadhyay, *J. Phys. Chem. B*, 2013, **117**, 6250–6255.
- 26 S. Mitra, V. K. Sharma, V. G. Sakai, A. Orecchini, T. Seydel, M. Johnson and R. Mukhopadhyay, *J. Phys. Chem. B*, 2016, **120**, 3777.
- 27 O. Holderer, H. Frielinghaus, M. Monkenbusch, M. Klostermann, T. Sottmann and D. Richter, *Soft Matter*, 2013, **9**, 2308.
- 28 S. Wellert, H.-J. Altmann, A. Richardt, A. Lapp, P. Falus, B. Farago and T. Hellweg, *Eur. Phys. J. E: Soft Matter Biol. Phys.*, 2010, **33**, 243–250.
- 29 V. K. Sharma, H. Srinivasan, S. Mitra, V. Garcia-Sakai and R. Mukhopadhyay, *J. Phys. Chem. B*, 2017, **121**, 5562–5572.
- 30 M. Saxton, *Curr. Top. Membr.*, 1999, **48**, 229–282.
- 31 J. C. Lopez-Montilla, S. Pandey, D. O. Shah and O. D. Crisalle, *Water Res.*, 2005, **39**(9), 1907–1913.
- 32 K. V. Schubert, R. Strey, S. R. Kline and E. W. Kaler, *J. Chem. Phys.*, 1994, **101**, 5343–5355.
- 33 J. R. D. Copley and J. C. Cook, *Chem. Phys.*, 2003, **292**, 477–485.
- 34 R. T. Azuah, L. R. Kneller, Y. Qiu, P. L. W. Tregenna-Piggott, C. M. Brown, J. R. D. Copley and R. M. Dimeo, *J. Res. Natl. Inst. Stand. Technol.*, 2009, **114**, 341.
- 35 S. Maccarrone, D. V. Byelov, T. Auth, J. Allgaier, H. Frielinghaus, G. Gompper and D. Richter, *J. Phys. Chem. B*, 2013, **117**, 5623–5632.
- 36 G. Gompper, H. Endo, M. Mihailescu, J. Allgaier, M. Monkenbusch, D. Richter, B. Jakobs, T. Sottmann and R. Strey, *Europhys. Lett.*, 2001, **56**, 683.
- 37 S. Engelskirchen, N. Elsner, T. Sottmann and R. Strey, *J. Colloid Interface Sci.*, 2007, **312**, 114–121.
- 38 V. K. Sharma, S. Mitra, V. Garcia Sakai, P. A. Hassan, J. Peter Embs and R. Mukhopadhyay, *Soft Matter*, 2012, **8**, 7151–7160.
- 39 S. Busch, C. Smuda, L. C. Pardo and T. Unruh, *J. Am. Chem. Soc.*, 2010, **132**, 3232–3233.
- 40 M. Doxastakis, V. Garcia Sakai, S. Ohtake, J. K. Maranas and J. J. de Pablo, *Biophys. J.*, 2007, **92**, 147–161.
- 41 R. E. Lechner, *Solid State Ionics*, 1995, **77**, 280–286.
- 42 M. A. Barrett, M. Trapp, W. Lohstroh, T. Seydel, J. Ollivier, M. Ballauff, N. A. Dencherd and T. Hauß, *Soft Matter*, 2016, **12**, 1444–1451.
- 43 V. K. Sharma, E. Mamontov, D. B. Anunciado, H. O'Neill and V. Urban, *J. Phys. Chem. B*, 2015, **119**, 4460–4470.
- 44 L. Topozini, C. L. Armstrong, M. A. Barrett, S. Zheng, L. Luo, H. Nanda, V. G. Sakai and M. C. Rheinstädter, *Soft Matter*, 2012, **8**, 11839–11849.
- 45 H. Nėry, O. Sėderman, D. Canet, H. Walderbaug and B. Lindmant, *J. Phys. Chem.*, 1986, **90**, 5802–5808.
- 46 F. Volino and A. J. Dianoux, *Mol. Phys.*, 1980, **41**, 271–279.
- 47 V. K. Sharma, E. Mamontov, M. Tyagi, S. Qian, D. K. Rai and V. S. Urban, *J. Phys. Chem. Lett.*, 2016, **7**, 2394–2401.
- 48 V. K. Sharma, E. Mamontov, D. B. Anunciado, H. O'Neill and V. S. Urban, *Soft Matter*, 2015, **11**, 6755–6767.
- 49 V. K. Sharma, E. Mamontov, M. Tyagi and V. S. Urban, *J. Phys. Chem. B*, 2016, **120**, 154–163.
- 50 V. K. Sharma, E. Mamontov, M. Ohl and M. Tyagi, *Phys. Chem. Chem. Phys.*, 2017, **19**, 2514–2524.
- 51 D. K. Rai, V. K. Sharma, D. Anunciado, H. O'Neill, E. Mamontov, V. Urban, W. T. Heller and S. Qian, *Sci. Rep.*, 2016, **6**, 30983.